Single-molecule DNA repair in live bacteria

Stephan Uphoff[a,1], Rodrigo Reyes-Lamothe[b], Federico Garza de Leon[a], David J. Sherratt[c], and Achillefs N. Kapanidis[a,1]

[a]Biological Physics Research Group, Clarendon Laboratory, Department of Physics, University of Oxford, Oxford OX1 3PU, United Kingdom; [b]Department of Biology, McGill University, Montreal, Quebec, Canada H3G 0B1; and [c]Microbiology Unit, Department of Biochemistry, University of Oxford, Oxford OX1 3QU, United Kingdom

Cellular DNA damage is reversed by balanced repair pathways that avoid accumulation of toxic intermediates. Despite their importance, the organization of DNA repair pathways and the function of repair enzymes in vivo have remained unclear because of the inability to directly observe individual reactions in living cells. Here, we used photoactivation, localization, and tracking in live *Escherichia coli* to directly visualize single fluorescent labeled DNA polymerase I (Pol) and ligase (Lig) molecules searching for DNA gaps and nicks, performing transient reactions, and releasing their products. Our general approach provides enzymatic rates and copy numbers, substrate-search times, diffusion characteristics, and the spatial distribution of reaction sites, at the single-cell level, all in one measurement. Single repair events last 2.1 s (Pol) and 2.5 s (Lig), respectively. Pol and Lig activities increased fivefold over the basal level within minutes of DNA methylation damage; their rates were limited by upstream base excision repair pathway steps. Pol and Lig spent >80% of their time searching for free substrates, thereby minimizing both the number and lifetime of toxic repair intermediates. We integrated these single-molecule observations to generate a quantitative, systems-level description of a model repair pathway in vivo.

single-molecule tracking | super-resolution microscopy | DNA damage response | protein-DNA interaction | cytosolic diffusion

All cellular organisms rely on complex DNA repair mechanisms for faithful chromosome replication and maintenance of their genome integrity (1). The variety of DNA lesions requires modular repair pathways that carry out damage recognition, damage removal, repair synthesis, and ligation in sequential steps catalyzed by a series of enzymes. However, all repair pathway steps need to be precisely balanced to avoid accumulation of DNA intermediates that are typically more mutagenic and toxic than the original lesion (2). Rapid processing of gapped and nicked intermediates is particularly crucial (3) because they provoke lethal double-strand breaks upon encountering replication forks (4); a single such break can lead to chromosome loss and cell death.

Despite extensive genetic, biochemical, and biophysical studies (1), the molecular organization of DNA repair in vivo remains unclear. Most of our mechanistic understanding relies on in vitro ensemble studies, which cannot replicate the cellular environment and stochastic nature of chemical reactions. By avoiding ensemble-averaging, single-molecule experiments have revolutionized the study of protein–DNA interactions in vitro, but extension of these powerful concepts to DNA repair measurements in living cells remains an open goal. Early in vivo work focused on the mean behavior of cell populations and could not examine functionally important heterogeneity, such as the variation in protein copy numbers between cells and over time (5, 6). Such variation can lead to different repair rates across genetically identical cells and may derail coordination between steps within the pathway, especially following DNA damage responses. Single-cell fluorescence studies can address some of these issues, but their limited resolution has left the detailed spatial distribution of the repair machinery under debate (7–9). Although many molecular processes in eukaryotes show a high degree of spatial organization, as exemplified by the observation of "factories" of DNA replication, transcription, and repair (10), the existence and functional role of spatially organized protein activity in bacteria is still controversial. Further, cellular DNA repair mechanisms have been characterized mainly by deleting pathway components or altering their expression (3, 11–13).

However, reaction pathways are not defined solely by protein concentrations, but by reaction rates that depend on protein and substrate concentrations and enzymatic rates in the cell. Consequently, describing repair pathways quantitatively has proven difficult, because the rates are either unknown or have to be obtained from various in vitro experiments performed under different conditions (14, 15). Hence there is a need to quantify rates at the single-cell level and relate them to the concentrations and spatial distribution of substrates and repair proteins as well as to the timing of individual reactions and search processes.

To address these objectives, we developed a general single-molecule fluorescence method to directly visualize repair reactions in individual live *Escherichia coli* cells. We studied base excision repair (BER) of DNA-methylation damage by methyl methanesulfonate (MMS), which generates single-nucleotide gap intermediates (16). We focused on the final two BER steps, both conserved from bacteria to humans and across repair pathways: DNA synthesis by DNA polymerase I (Pol) and subsequent nick ligation by DNA ligase (Lig; Fig. 1A) (11, 12); these reactions also link Okazaki fragments in lagging-strand DNA replication (17). Pol and Lig have been extensively characterized as model enzymes in vitro, but their actual cellular activities have not been directly observed and quantified. Fluorescence microscopy is well suited for this task (18), but is limited by its current spatial and temporal resolution. Fluorescence recovery after photobleaching experiments have revealed global DNA repair kinetics in eukaryotes (19, 20), but this model-dependent approach cannot easily resolve molecular subpopulations to extract binding and diffusion constants. Although single fluorescent proteins can be detected in live bacteria (21, 22), they typically report on only a few labeled molecules per cell. Attempts to visualize lagging-strand replication by fluorescent-labeled Pol molecules (~400 copies/cell) (1, 17) showed a broad diffraction-limited distribution in *E. coli* (Fig. 1B) (22). To detect single reactions directly, we imaged molecules sequentially using photoactivated localization microscopy (PALM) (23–25) combined with single-molecule tracking (26–28) of photoactivatable mCherry (PAmCherry) fusion proteins (29). This approach provided an unprecedented comprehensive dataset of Pol and Lig reaction rates, substrate search times, and diffusion coefficients as well as the number, localization, and lifetime of DNA damage sites in live *E. coli*. We quantified dynamic changes of these observables during the damage response and adaptation.

Results

PALM Tracking of Fluorescent Fusions. We replaced endogenous genes with C-terminal PAmCherry fusions (*SI Appendix,* Table S1). The growth rates and MMS sensitivity of the fusion strains were identical to WT (*SI Appendix,* Table S2), whereas a temperature-sensitive Pol mutant strain exhibited hypersensitivity to

Fig. 1. PALM and tracking of DNA-binding proteins in live *E. coli*. (*A*) Excision repair pathways leave gapped intermediates to be filled by DNA polymerase and sealed by Lig. (*B*) Accumulated Pol-PAmCherry fluorescence in a live *E. coli* cell. (Scale bars, 1 μm.) (*C*) PSF of a single Pol-PAmCherry molecule at 15-ms exposure. (*D*) Example tracks of diffusing Pol (blue) and bound Pol (red) on a transmitted light image. (*E*) All Pol tracks in one cell. (*F*) Pol tracks label the nucleoid in replicating *E. coli*. Tracks are shown on transmitted light images with the distribution of localizations across the long cell axis. (*Left* to *Right*): short cell with a single chromosome; medium-length cell during chromosome segregation; long cell with two separated chromosomes. (*G*) MSD versus lag time (± SD) for Fis (green triangles), Lig (black triangles), Pol (blue circles) in live cells, and Pol in fixed cells (red squares). (*H*) Cumulative distributions of the diffusion step length between consecutive localizations. The distributions shift to longer steps with increasing diffusion coefficient *D*.

MMS (*SI Appendix*, Fig. S1). We measured live cells immobilized on agarose under continuous 561-nm excitation; >95% of cells remained viable after imaging (*SI Appendix*, Fig. S1). By controlling 405-nm photoactivation, we imaged less than one fluorophore per cell at any time (Fig. 1*C*, Movie S1), giving a clear fluorescent point-spread-function (PSF) in 15-ms exposures. We tracked consecutive localizations to follow the movement of single molecules until irreversible photobleaching (Fig. 1 *D* and *E*).

Pol and Lig in Undamaged Cells. We first inspected Pol and Lig tracks in the absence of exogenous DNA damage. The spatial distribution of tracks reflected the structure of the nucleoid in replicating *E. coli* (30) (Fig. 1*F* and *SI Appendix*, Fig. S2). In short cells with a single chromosome, Pol tracks occupied the central area of the cell, avoiding the poles. Increasing cell length correlated with the progression of chromosome replication and segregation, as evident from the presence of two distinct areas of high Pol density in cells of intermediate length; these two areas separated entirely in the longest cells before the appearance of a constricting septum that marks cell division.

Mean-squared displacement (MSD) curves from tracks in live cells rise linearly but saturate at long lag times because of confinement within the nucleoid (Fig. 1*G*). We measured the small nucleoid-associated protein Fis (31) for comparison. The step lengths between consecutive localizations scaled with the expected molecular weights (Fig. 1*H*): 76-kDa Fis dimers showed the fastest diffusion, followed by 102-kDa Lig and 136-kDa Pol (molecular weights include 27 kDa per PAmCherry). These results confirmed integrity of the fusion proteins and show that Pol and Lig do not stably form larger replication or repair complexes in the cytoplasm. Pol displacements in fixed cells (red curve in Fig. 1*H*) represent the 40-nm localization precision.
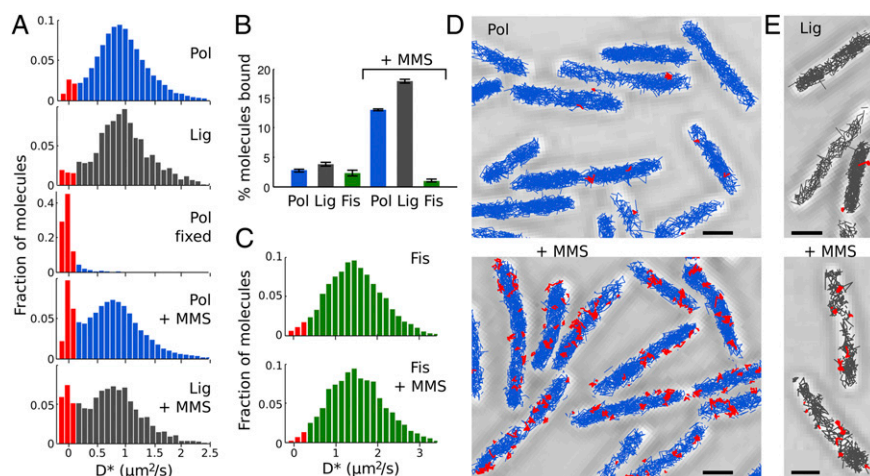
We asked if subpopulations of Pol and Lig were active in lagging strand replication and basal DNA repair. We hypothesized that molecules performing reactions while bound to DNA might have a significantly lower diffusion coefficient than free Pol and Lig, which are both expected to show only weak, nonspecific DNA-binding (*SI Appendix*), and considering that chromosomal DNA loci have a low diffusion coefficient of ~10^{-5} μm^2·s^{-1} (32). Our single-molecule approach can reveal such molecular heterogeneity by measuring the apparent diffusion coefficient *D** of each track: $D^* = MSD/(4 \Delta t) - \sigma_{loc}^2/\Delta t$ (correcting for the localization error

σ_{loc}). Undamaged cells showed primarily diffusing Pol and Lig with distributions centered at *D** ~0.8 μm^2·s^{-1} and ~1 μm^2·s^{-1}, respectively (Fig. 2*A*). In contrast, fixed cells contained almost exclusively Pol molecules that appeared immobile, as expected (Fig. 2*A*). Using a threshold on *D** (based on the fixed cells control and simulations), we identified populations of 2.7 ± 0.2% and 3.8 ± 0.4% bound Pol and Lig with *D** ~0 μm^2·s^{-1}, respectively (red bars in Fig. 2*A*). As a positive control for our ability to identify single DNA-bound proteins against the pool of unbound molecules, we imaged DNA Pol III-PAmCherry (ε subunit), exploiting the known positioning of replication forks in the cell (22). As expected, tracks of bound Pol III localized exclusively at midcell or at symmetric positions in each cell half; in contrast, tracks of diffusing molecules were distributed throughout the cell (*SI Appendix*, Fig. S3).

We performed simulations to characterize the observed motion of Pol and Lig. Instead of simulating the final trajectories directly (27, 28), we fully modeled PALM movies of Brownian motion within the nucleoid, including the distinct populations of bound Pol and Lig molecules (*SI Appendix*, Fig. S4; *SI Appendix*). We found that simulations with diffusion coefficients $D_{Pol} = 2.7 \pm 0.4$ μm^2·s^{-1} and $D_{Lig} = 3.5 \pm 0.3$ μm^2·s^{-1} precisely matched our experimental results (*SI Appendix*, Fig. S4). Note that apparent diffusion coefficients (*D**) are lower than these values because of the confinement and motion blurring (33). The close agreement between simulation and experiment suggests that Pol and Lig perform effective Brownian motion. Although the nucleoid association indicates nonspecific DNA interactions, the displacement between subsequent localizations limits transient DNA binding to <15 ms, excluding substrate search processes wherein Pol and Lig processively scan long chromosomal segments, as shown for other repair proteins in vitro (34, 35). The observed Brownian motion (i.e., Gaussian distribution of step lengths) likely results from a sum of multiple displacements and nonspecific binding events per frame.

Direct Observation of DNA Repair. To test whether the bound populations of Pol and Lig represent molecules performing DNA synthesis and ligation, we generated single-nucleotide gap substrates in vivo, using BER of exogenous DNA-methylation damage. MMS treatment of live cells for 20 min resulted in fivefold increased bound-molecule fractions: 13.0 ± 0.2% bound Pol and 17.9 ± 0.3% bound Lig (Fig. 2 *A* and *B*). The DNA-binding

Fig. 2. Direct observation of DNA repair in live *E. coli*. (*A*) Distributions of the apparent diffusion coefficient (*D**) for Pol and Lig in undamaged cells; Pol in fixed cells; Pol and Lig in live cells under constant 100-mM MMS treatment. *n* > 2,000 tracks; bound molecule populations are shown in red. (*B*) Percentage of bound Pol, Lig, and Fis molecules in undamaged cells and with MMS (± SEM; *n* > 2,000 tracks). (*C*) *D** distributions for Fis in undamaged cells and with 100 mM MMS treatment (*n* > 10,000 tracks). (*D* and *E*) Pol and Lig tracks in undamaged cells (*Upper*) and with MMS (*Lower*). Diffusing tracks in blue/gray, bound tracks in red. (Scale bars, 1 μm.)

protein Fis served as a control without DNA repair activity, showing no increase in binding with MMS (Fig. 2*C* and *SI Appendix*, Fig. S3). Because the MMS response was specific to the two DNA repair proteins, we interpret the tracks of single bound Pol and Lig molecules as direct reports of DNA synthesis and ligation reactions (red tracks in Fig. 2 *D* and *E*; Movie S2). Notably, the spatial organization and *D** distributions of free Pol and Lig were similar with and without MMS, suggesting that their global diffusion and search processes did not change significantly within 20 min of DNA damage. By examining the locations of bound tracks, we found that the repair sites were spread throughout the cell, matching the spatial distribution of free Pol and Lig (*SI Appendix*, Fig. S5). This supports a distributive search model of individual Pol and Lig molecules for damage sites on the chromosome, instead of these sites being directed to spatially organized "repair factories" (7), as suggested for human cells and mitochondria (8, 9). Our results validate the common assumption of a uniform distribution of damage sites in computer models of DNA repair in *E. coli* (14, 15).

DNA Repair Times. To directly visualize complete substrate search and repair cycles, we identified individual tracks that showed free diffusion leading to a binding event, followed by dissociation and continued diffusion (Fig. 3 *A–C* and *SI Appendix*, Fig. S6). Corresponding time-traces of the stochastic diffusion steps displayed characteristic binding intervals with *D** ~0 μm²·s⁻¹. The bound population is hence in dynamic exchange with the pool of diffusing molecules. However, most molecules remained either in the diffusing or bound state for the entire track, limited by photobleaching. To minimize the influence of photobleaching on the apparent repair times, we used longer exposures with low excitation intensities and sparse photoactivation. Under these conditions, PSFs of diffusing molecules were dim and blurred (because of motion during exposure), but PSFs of bound molecules remained narrow (Fig. 3 *D* and *E*). Because the population of narrow PSFs increased with MMS (red bars in Fig. 3*F* and *SI Appendix*, Fig. S7), we interpret the exponentially distributed Pol and Lig binding times as repair times $t_{Pol} = 2.1 \pm 0.3$ s and $t_{Lig} = 2.5 \pm 0.4$ s (Fig. 3 *G* and *H* and *SI Appendix*, Fig. S7 and Table S3). Binding times in undamaged cells matched those under MMS treatment, suggesting that the rate-limiting steps are the same for lagging-strand replication and repair reactions. The total Pol repair time includes filling the single-nucleotide gap and potential strand displacement synthesis at a rate of >10 nt/s (36), followed by nuclease cleavage of the generated 5′ flap and product release; the latter is the likely single rate-limiting step. Our in vivo result is in agreement with the ~2-s binding time of Klenow fragment (large domain of Pol) to a DNA primer in vitro (37). The Lig repair time corresponds to the ligation reaction and product release and is consistent with the in vitro measurement of 2.4 s (38). Despite this

agreement, in vitro studies can make only limited predictions about reaction rates in the cell because binding affinities are strongly influenced by salt and substrate concentrations and macromolecular crowding.

DNA Repair Rates. To convert reaction times into reaction rates that include the search time t_{search} for a substrate, we used the measured fraction of bound molecules: $N_{bound}/(N_{bound} + N_{free}) = t_{bound}/(t_{bound} + t_{search})$. This gives the reaction rate per molecule: $1/(t_{bound} + t_{search})$. We found that single Pol and Lig have basal reaction rates of ~0.7 min⁻¹ and ~0.9 min⁻¹ in undamaged cells. The total cellular repair rates depend linearly on the protein copy number. PALM can be used to directly count molecules at the single-cell level, considering that each PAmCherry fluorophore is activated once (29). We counted 479 Pol, 226 Lig, and 1,560 Fis copies/cell (median values; Fig. 4*A* and *SI Appendix*, Fig. S8). These numbers are in agreement with previous reports of ~400 Pol (17), ~200 Lig (1), and thousands of Fis (31).

Using the median copy numbers, we estimated cellular reaction rates of ~330 min⁻¹ for Pol and ~210 min⁻¹ for Lig (Table 1). The basal activities match expectations: DNA replication accounts for 35–60% of the observed rates, considering two replication forks per cell-generating Okazaki fragments at a rate of ~120 min⁻¹ (17). Additionally, Pol and Lig are involved in the repair of replication errors and damage by reactive metabolites, including endogenous methylating agents (1, 16). Normal metabolism causes 3,000–5,000 lesions per *E. coli* generation by oxidative DNA damage alone, requiring a repair rate of 25–40 min⁻¹ (39). Under MMS treatment, the reaction rates increased to ~3.7 min⁻¹ and ~5.1 min⁻¹ per single Pol and Lig, leading to cellular repair rates of ~1,780 min⁻¹ and ~1,150 min⁻¹, respectively (Table 1); the 50% higher Pol activity over Lig likely reflects the wider range of Pol substrates and its nick-translation activity, which competes with ligation (40). As the final step in the pathway, the Lig activity corresponds to the overall BER rate.

Pol and Lig Activities Are Limited by Substrate Availability. Single-cell analysis uncovered significant variation in repair activities across cells, with distributions ranging from 0% to 40% bound Pol and Lig (Fig. 4*B*). We examined four factors that may influence the observed rates and their variation: Pol and Lig copy numbers, MMS concentration, upstream reactions in the BER pathway, and MMS treatment time. To test the influence of Pol and Lig copy numbers, we measured DNA-binding and protein counts simultaneously at the single-cell level. By linking the natural copy number variation between cells with the bound-fraction distribution across cells, we found that the percentage of bound Pol and Lig was lower in cells with higher copy numbers but similar size (Fig. 4*C*). In those cells, the excess copies joined the diffusing pool of molecules and the total number of bound
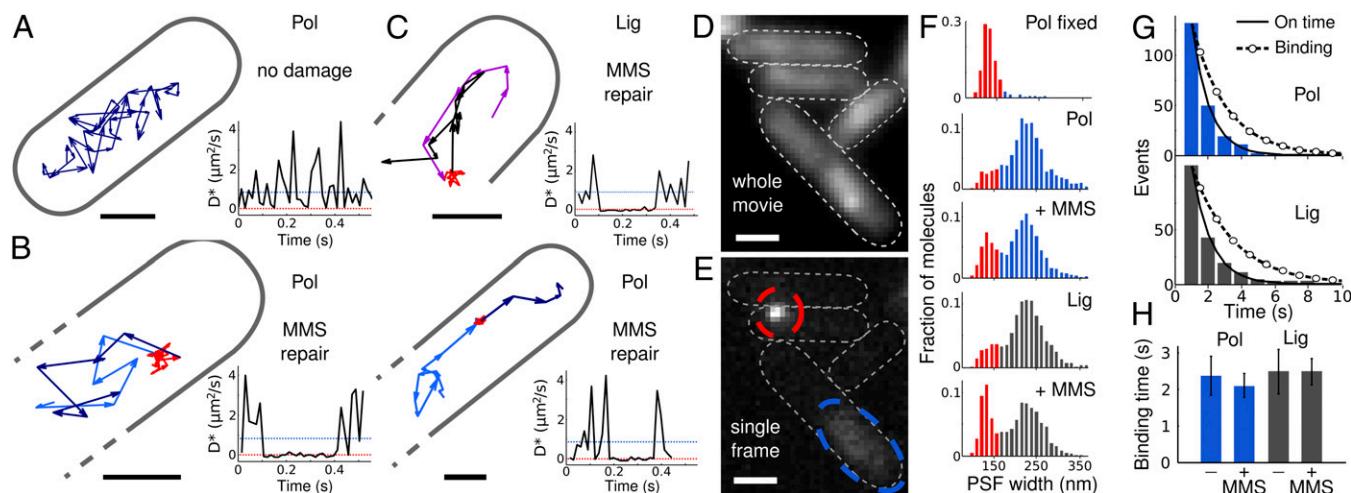
Fig. 3. Visualizing and timing individual repair events. (*A*) Single Pol track in an undamaged cell. (Scale bars, 0.5 μm.) Time trace of the corresponding diffusion steps from the displacements between localizations; dotted blue and red lines are the average *D** of free and bound Pol, respectively. (*B*) Two example Pol tracks in MMS damaged cells showing the substrate search path (light blue) that leads to a repair event (red), and continued search (dark blue). Corresponding time traces show *D** ~ 0 μm²·s⁻¹ during repair events. (*C*) Lig search (magenta), repair (red), and continued diffusion (black), with *D** time trace. (*D*) Accumulated Pol-PAmCherry fluorescence of a whole movie. (Scale bars, 1 μm.) (*E*) Example frame at 750-ms exposure time with PSFs of bound and diffusing Pol (red and blue outlines). (*F*) Fitted PSF width in fixed cells, undamaged cells, and with 100-mM MMS at 750-ms exposure time. Bound populations with narrow PSFs are in red. (*G*) On-time distributions for bound Pol and Lig with exponential fits (solid lines) and photobleaching-corrected binding time distributions (dashed circled lines). (*H*) Mean Pol and Lig binding times in undamaged cells and with MMS (± SEM; from three exposure and excitation conditions).

Pol and Lig molecules saturated at ~60 and ~40 bound molecules/cell, respectively (Fig. 4*D*). This demonstrates that Pol and Lig activities are limited by substrate sites available for binding.

Dose–response curves showed that Pol and Lig binding saturated with increasing MMS concentration (at ~13% and ~18% bound fraction, Fig. 4*E*). The Pol activity is therefore not limited by the initial damage, but instead by upstream BER steps, such as the glycosylase and nuclease reactions. Below saturating MMS concentrations, the steady-state ligation rate is expected to equal the rate at which lesions are generated. Based on previous in vitro and in vivo reports (41, 42), we estimated the damage rate by 25 mM MMS to ~430–460 lesions·chromosome⁻¹·min⁻¹, in agreement with our measured Lig rate of 469 ± 136 reactions·cell⁻¹·min⁻¹ at 25 mM MMS (*SI Appendix*). We measured the same trend of saturated Pol activity during the MMS response over time, with the bound Pol fraction increasing significantly in 5 min and

reaching a plateau at the limiting activity of ~13% binding after 15 min of treatment (red curve in Fig. 5*A*). We also explored the Pol response to brief MMS treatment followed by MMS removal, showing rapid reduction of Pol binding after 5 min and return close to basal activity within ~15 min of recovery (Fig. 5*B*); Pol catalyzed ~18,000 repair events per cell during the damage and recovery experiment (orange shaded area in Fig. 5*B*). Residual activity after the initial fast recovery may reflect slower repair of complicated lesions such as double-strand breaks (39, 43).

Pretreatment of *E. coli* with a low MMS dose induces the adaptive response, which up-regulates 3-methyladenine DNA glycosylase II, rendering cells more resistant to subsequent higher doses (1, 16). Adapted cells showed the same timing of Pol activity during the initial MMS response as nonadapted cells, but saturation occurred at a higher value of ~19% binding (cellular repair rate ~2,500 min⁻¹; magenta curve in Fig. 5*A*). Increased repair
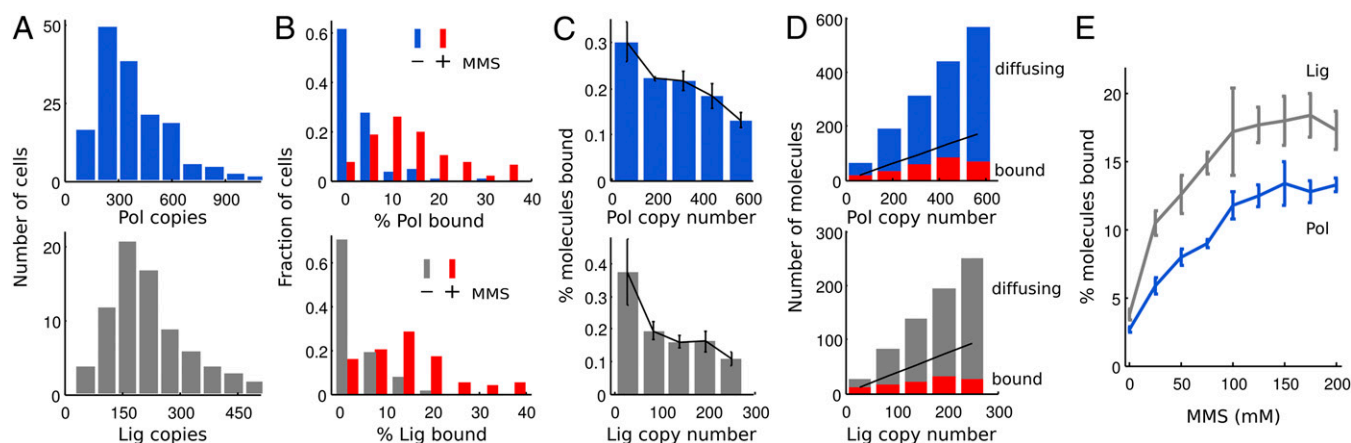
Fig. 4. Single-cell analysis shows that Pol (*Upper* row) and Lig (*Lower* row) saturate repair substrates. (*A*) Protein copy number distributions. (*B*) Distributions of the percentage of bound Pol and Lig across cells in undamaged cells and with 100-mM MMS. (*C*) Percentages of bound Pol and Lig with MMS as a function of their copy numbers per cell (± SEM). (*D*) Number of diffusing and bound Pol and Lig with MMS as a function of their copy numbers per cell. Black lines: hypothetical case of unlimited substrates in which the bound percentage was independent of the copy number. (*E*) MMS dose–response curves show the average percentage of bound Pol and Lig for different MMS concentrations (± SEM; n = 4).
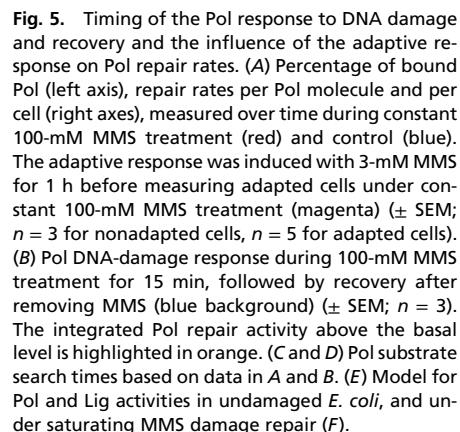
Table 1. Pol and Lig activities in undamaged cells and under saturating MMS damage

Experiment	% bound	Bound molecules, cell⁻¹	Binding time, s	Search time, s	Rate, molecule⁻¹·min⁻¹	Rate, cell⁻¹·min⁻¹
Pol	2.7 ± 0.2	13 ± 1	2.4 ± 0.5	85 ± 20	0.7 ± 0.2	329 ± 76
Lig	3.8 ± 0.4	9 ± 1	2.5 ± 0.6	63 ± 17	0.9 ± 0.2	207 ± 54
Pol MMS	13.0 ± 0.2	62 ± 1	2.1 ± 0.3	14 ± 2	3.7 ± 0.5	1,782 ± 248
Lig MMS	17.9 ± 0.3	40 ± 1	2.5 ± 0.4	9 ± 2	5.1 ± 0.7	1,152 ± 167

Bound molecules and rates per cell are stated for exact copy numbers of 479 Pol and 226 Lig (median values in Fig. 4A). Errors are ± SEM for % bound and binding times; other errors were estimated by error propagation. Variation in copy numbers will introduce additional variation in the number of bound molecules and rates per cell.

initiation in adapted cells hence propagates through the pathway to enhance the overall BER rate and modulate the Pol activity that is limited by upstream pathway steps. We noticed that adaptation slowed the diffusion of free Pol and confined tracks to a smaller area in the cell (*SI Appendix*, Fig. S9); this observation indicates a global nucleoid compaction that might facilitate repair and physically protect the chromosome against damage (44).

Substrate Search Times. Binding times and reaction rates also inform about the search time t_{search} between subsequent reactions. Dictated by the availability of free substrates, t_{search} decreased from ~85 s for Pol in undamaged cells to ~14 s with saturating MMS damage, and increased again during recovery (Fig. 5 *C* and *D*). Even at maximum BER activity, Pol and Lig spent >80% of time searching for free substrates. Using the relation between the diffusion-limited association rate (45) and search times, we estimated four to five free gaps or nicks with lifetimes of ~140 ms and ~90 ms, respectively, to be present at any time with saturating MMS; this contrasts to 62 Pol-bound and 40 Lig-bound substrates. The short lifetime of free gaps and nicks, a consequence of the distributive search by excess numbers of Pol and

Lig, minimizes accumulation of these repair intermediates and safeguards genomic stability.

Discussion

DNA synthesis and ligation are essential steps in base excision, nucleotide excision, and mismatch repair pathways of all cellular organisms. Here, we presented a direct view on DNA repair and generated a quantitative systems-level account of a model reaction pathway in vivo (Table 1 and Fig. 5 *E* and *F*). Individual Pol and Lig molecules diffuse with little affinity for undamaged DNA but become transiently immobilized for repair on randomly distributed damage sites. Although Pol and Lig mutants are hypersensitive to DNA damage (11, 12), only a small percentage of WT activity appears to be required for normal growth (1, 17). Indeed, we showed that 2.7% of ~400 Pol and 3.8% of ~200 Lig copies per cell are active in replication and basal repair at any time. However, excess copies become important under severe exogenous damage, processing up to ~1,150 gapped intermediates per cell per minute.

Cells benefit from high Pol and Lig capacities relative to repair initiation because gapped and nicked intermediates are more toxic than the predominant 7-methylguanine lesions caused by

Fig. 5. Timing of the Pol response to DNA damage and recovery and the influence of the adaptive response on Pol repair rates. (*A*) Percentage of bound Pol (left axis), repair rates per Pol molecule and per cell (right axes), measured over time during constant 100-mM MMS treatment (red) and control (blue). The adaptive response was induced with 3-mM MMS for 1 h before measuring adapted cells under constant 100-mM MMS treatment (magenta) (± SEM; n = 3 for nonadapted cells, n = 5 for adapted cells). (*B*) Pol DNA-damage response during 100-mM MMS treatment for 15 min, followed by recovery after removing MMS (blue background) (± SEM; n = 3). The integrated Pol repair activity above the basal level is highlighted in orange. (*C* and *D*) Pol substrate search times based on data in A and B. (*E*) Model for Pol and Lig activities in undamaged *E. coli*, and under saturating MMS damage repair (*F*).

MMS (2). Abundance of high-fidelity Pol also favors competition against ~200 copies per cell of error-prone DNA Pol IV to lower mutagenesis associated with DNA repair (7, 43). Finally, gene expression noise and damage responses challenge the pathway balance and overall repair rates; excess amounts of Pol and Lig ensure sufficient repair capacities even in cells that contain relatively fewer copies.

Our approach can be used to elucidate a wide range of molecular processes in vivo (46). In principle, it allows quantification of reaction rates for any enzyme that changes diffusion characteristics upon substrate binding and release. Our results provide a starting point for quantitative modeling of entire repair pathways toward predicting an organism's response to DNA damage.

Materials and Methods

Details on materials and methods are available in the *SI Appendix*. In brief, *E.coli* AB1157 endogenous PAmCherry fusions were created by λ-Red recombination. Cells were grown in M9 minimal medium to OD ~0.1 and immobilized for imaging on 1% agarose pads, containing 100 mM MMS (Sigma) for DNA damage experiments (different concentrations in Fig. 4*E*).

A custom single-molecule fluorescence microscope with 405-nm (CNI) photoactivation and 561-nm (Oxxius) excitation lasers was used to record PALM movies on an EMCCD camera (Andor) at 15.26 ms/frame for 7,500–10,000 frames. Data analysis and simulations were performed in MATLAB (Math-Works). PSFs were localized to 40-nm precision by elliptical Gaussian fitting. Localizations within a radius of 0.57 μm in consecutive frames were linked to tracks. Tracks with more than four steps were used to compute apparent diffusion coefficients (D^*). Bound molecules were identified using two thresholds: $D^* < 0.15\ \mu m^2 \cdot s^{-1}$ for MSD($\Delta t = 15$ ms) and $D^* < 0.075\ \mu m^2 \cdot s^{-1}$ for MSD($\Delta t = 30$ ms). Protein copy number distributions were obtained from the number of tracks per cell.

1. Friedberg EC (2006) *DNA Repair and Mutagenesis* (American Society for Microbiology, Washington, DC).
2. Fu D, Calvo JA, Samson LD (2012) Balancing repair and tolerance of DNA damage caused by alkylating agents. *Nat Rev Cancer* 12(2):104–120.
3. Senejani AG, et al. (2012) Y265C DNA polymerase beta knockin mice survive past birth and accumulate base excision repair intermediate substrates. *Proc Natl Acad Sci USA* 109(17):6632–6637.
4. Kuzminov A (2001) Single-strand interruptions in replicating chromosomes cause double-strand breaks. *Proc Natl Acad Sci USA* 98(15):8241–8246.
5. Elowitz MB, Levine AJ, Siggia ED, Swain PS (2002) Stochastic gene expression in a single cell. *Science* 297(5584):1183–1186.
6. Huh D, Paulsson J (2011) Random partitioning of molecules at cell division. *Proc Natl Acad Sci USA* 108(36):15004–15009.
7. Goodman MF (2002) Error-prone repair DNA polymerases in prokaryotes and eukaryotes. *Annu Rev Biochem* 71:17–50.
8. Jackson DA, Balajee AS, Mullenders L, Cook PR (1994) Sites in human nuclei where DNA damaged by ultraviolet light is repaired: Visualization and localization relative to the nucleoskeleton. *J Cell Sci* 107(Pt 7):1745–1752.
9. Stuart JA, Mayard S, Hashiguchi K, Souza-Pinto NC, Bohr VA (2005) Localization of mitochondrial DNA base excision repair to an inner membrane-associated particulate fraction. *Nucleic Acids Res* 33(12):3722–3732.
10. Cook PR (1999) The organization of replication and transcription. *Science* 284(5421):1790–1795.
11. Konrad EB, Modrich P, Lehman IR (1973) Genetic and enzymatic characterization of a conditional lethal mutant of Escherichia coli K12 with a temperature-sensitive DNA ligase. *J Mol Biol* 77(4):519–529.
12. Ljungquist S, Lindahl T, Howard-Flanders P (1976) Methyl methane sulfonate-sensitive mutant of Escherichia coli deficient in an endonuclease specific for apurinic sites in deoxyribonucleic acid. *J Bacteriol* 126(2):646–653.
13. Glassner BJ, Rasmussen LJ, Najarian MT, Posnick LM, Samson LD (1998) Generation of a strong mutator phenotype in yeast by imbalanced base excision repair. *Proc Natl Acad Sci USA* 95(17):9997–10002.
14. Ni M, Wang S-Y, Li J-K, Ouyang Q (2007) Simulating the temporal modulation of inducible DNA damage response in Escherichia coli. *Biophys J* 93(1):62–73.
15. Karschau J, et al. (2011) A matter of life or death: Modeling DNA damage and repair in bacteria. *Biophys J* 100(4):814–821.
16. Sedgwick B (2004) Repairing DNA-methylation damage. *Nat Rev Mol Cell Biol* 5(2):148–157.
17. Kornberg A (2005) *DNA Replication* (University Science Books, Herndon, VA).
18. Feuerhahn S, Egly J-M (2008) Tools to study DNA repair: What's in the box? *Trends Genet* 24(9):467–474.
19. Houtsmuller AB, et al. (1999) Action of DNA repair endonuclease ERCC1/XPF in living cells. *Science* 284(5416):958–961.
20. Politi A, et al. (2005) Mathematical modeling of nucleotide excision repair reveals efficiency of sequential assembly strategies. *Mol Cell* 19(5):679–690.
21. Elf J, Li G-W, Xie XS (2007) Probing transcription factor dynamics at the single-molecule level in a living cell. *Science* 316(5828):1191–1194.
22. Reyes-Lamothe R, Sherratt DJ, Leake MC (2010) Stoichiometry and architecture of active DNA replication machinery in Escherichia coli. *Science* 328(5977):498–501.
23. Betzig E, et al. (2006) Imaging intracellular fluorescent proteins at nanometer resolution. *Science* 313(5793):1642–1645.

24. Biteen JS, et al. (2008) Super-resolution imaging in live Caulobacter crescentus cells using photoswitchable EYFP. *Nat Methods* 5(11):947–949.
25. Huang B, Bates M, Zhuang X (2009) Super-resolution fluorescence microscopy. *Annu Rev Biochem* 78:993–1016.
26. Manley S, et al. (2008) High-density mapping of single-molecule trajectories with photoactivated localization microscopy. *Nat Methods* 5(2):155–157.
27. Niu L, Yu J (2008) Investigating intracellular dynamics of FtsZ cytoskeleton with photoactivation single-molecule tracking. *Biophys J* 95(4):2009–2016.
28. English BP, et al. (2011) Single-molecule investigations of the stringent response machinery in living bacterial cells. *Proc Natl Acad Sci USA* 108(31):E365–E373.
29. Subach FV, et al. (2009) Photoactivatable mCherry for high-resolution two-color fluorescence microscopy. *Nat Methods* 6(2):153–159.
30. Reyes-Lamothe R, Nicolas E, Sherratt DJ (2012) Chromosome replication and segregation in bacteria. *Annu Rev Genet* 46:121–143.
31. Ball CA, Osuna R, Ferguson KC, Johnson RC (1992) Dramatic changes in Fis levels upon nutrient upshift in Escherichia coli. *J Bacteriol* 174(24):8043–8056.
32. Elmore S, Müller M, Vischer N, Odijk T, Woldringh CL (2005) Single-particle tracking of oriC-GFP fluorescent spots during chromosome segregation in Escherichia coli. *J Struct Biol* 151(3):275–287.
33. Michalet X, Berglund AJ (2012) Optimal diffusion coefficient estimation in single-particle tracking. *Phys Rev E Stat Nonlin Soft Matter Phys* 85(6 Pt 1):061916.
34. Blainey PC, van Oijen AM, Banerjee A, Verdine GL, Xie XS (2006) A base-excision DNA-repair protein finds intrahelical lesion bases by fast sliding in contact with DNA. *Proc Natl Acad Sci USA* 103(15):5752–5757.
35. Gorman J, et al. (2012) Single-molecule imaging reveals target-search mechanisms during DNA mismatch repair. *Proc Natl Acad Sci USA* 109(45):E3074–E3083.
36. Schwartz JJ, Quake SR (2009) Single molecule measurement of the "speed limit" of DNA polymerase. *Proc Natl Acad Sci USA* 106(48):20294–20299.
37. Markiewicz RP, Vrtis KB, Rueda D, Romano LJ (2012) Single-molecule microscopy reveals new insights into nucleotide selection by DNA polymerase I. *Nucleic Acids Res* 40(16):7975–7984.
38. Modorich P, Lehman IR (1973) Deoxyribonucleic acid ligase. A steady state kinetic analysis of the reaction catalyzed by the enzyme from Escherichia coli. *J Biol Chem* 248(21):7502–7511.
39. Cox MM (1998) A broadening view of recombinational DNA repair in bacteria. *Genes Cells* 3(2):65–78.
40. Sung J-S, Mosbaugh DW (2003) Escherichia coli uracil- and ethenocytosine-initiated base excision DNA repair: Rate-limiting step and patch size distribution. *Biochemistry* 42(16):4613–4625.
41. Fundador E, Rusling J (2007) Detection of labeled abasic sites in damaged DNA by capillary electrophoresis with laser-induced fluorescence. *Anal Bioanal Chem* 387(5):1883–1890.
42. Lossius I, Krüger PG, Kleppe K (1980) Effect of methyl methanesulfonate on the nucleoid structure of Escherichia coli. *J Gen Microbiol* 124:159–171.
43. Hastings PJ, et al. (2010) Competition of Escherichia coli DNA polymerases I, II and III with DNA Pol IV in stressed cells. *PLoS ONE* 5(5):e10862.
44. Levin-Zaidman S, et al. (2000) Ordered intracellular RecA-DNA assemblies: A potential site of in vivo RecA-mediated activities. *Proc Natl Acad Sci USA* 97(12):6791–6796.
45. Halford SE, Marko JF (2004) How do site-specific DNA-binding proteins find their targets? *Nucleic Acids Res* 32(10):3040–3052.
46. Badrinarayanan A, Reyes-Lamothe R, Uphoff S, Leake MC, Sherratt DJ (2012) In vivo architecture and action of bacterial structural maintenance of chromosome proteins. *Science* 338(6106):528–531.